SITE-SPECIFIC MANAGEMENT FOR BIOMASS FEEDSTOCK PRODUCTION: DEVELOPMENT OF REMOTE SENSING DATA ACQUISITION SYSTEMS

T. Ahamed

Energy Biosciences Institute, University of Illinois at Urbana-Champaign

L. Tian, Y. Zhang, Y. Xiong, B. Zhao, Y. Jiang, KC Ting

Department of Agricultural and Biological Engineering
University of Illinois at Urbana-Champaign

ABSTRACT

Efficient biomass feedstock production supply chain spans from site-specific management of crops on field to the gate of biorefinery. Remote sensing data acquisition systems have been introduced for site-specific management, which is a part of the engineering solutions for biomass feedstock production. A stand alone tower remote sensing platform was developed to monitor energy crops using multispectral imagery. The sensing system was capable of collecting RGB and CIR images during the crop growing season and transferring the images through a wireless network. A Lab View-based control algorithm has been developed to control the camera gain and exposure time under different illumination conditions. In addition, the horizontal and vertical rotation of pan tilt is controlled from a remote computer using a wireless network. A digital compass was installed with this system to get yaw and pitch orientations of the camera. A Data Acquisition Vehicle (DAV) has been built for crop close proximity measurements using a hyper-spectral camera and plant sample acquisitions. The vehicle employs a 4-wheel-drive-4-wheel-steering locomotion mechanism, and the vertical clearance is adjustable from 3 m to 4 m in responding to the different heights of various energy crops. The high spectral, spatial, and temporal resolutions from real-time image acquisitions are the advantages as compared to aerial and satellite imagery. The goal of this research is to explore the optimum harvest window for quality assurance of different biomass feedstock. Therefore, the experimental field has been laid out for monitoring Corn, Miscanthus, Switch grass, and Prairie grass simultaneously. N rate, K level, water stress, biomass yield, and energy content of each crop were compared using the remote sensing system. In addition, an Unmanned Aerial Vehicle (UAV) has been selected to capture images from low altitude to cover a wide range of fields on the biomass feedstock production farm.

Keywords: Energy Crops; Stand-alone Remote Sensing; Ground Reference Sensing; UAV Image Sensing, Biomass Yield

INTRODUCTION

Site-specific crop management is based on the fact that crop productivity varies spatially and temporarily within a field, depending on soil parameters, environmental conditions and operational activities (Bajwa and Tian). Precision agricultural technologies and processes have enhanced agricultural production for traditional crops like corn and soybeans; those techniques can now be adapted for the site-specific management of biomass feedstock. Biomass feedstock production is a critical subsystem within the overall biological energy production and utilization system that provides necessary material inputs for converting biomass into fuel, power, and value-added materials. This subsystem includes agronomic production of energy crops, physical handling and delivery of biomass, and other enabling logistics (Ting et al., 2008). Agronomic production depends on yield variability over the growing season to utilize the optimum harvesting window. Monitoring the yield variability of biomass feedstock is therefore essential for developing and evaluating site-specific crop management practices for perennial growth. Ground-based monitoring systems and data acquisition platforms must be developed based on airborne remote sensing technologies. Therefore, the objectives of this research are to develop optimized instrumentation and data processing systems to monitor the perennial growth of biomass feedstock and to identify crop stress as well as to develop algorithms for scheduling field operations. This paper describes the development and implementation of an optimized instrument for assessing biomass production. The first of three sections details activities related to a ground-based sensing, ground-referenced data collection vehicle (DAV) and an Unmanned Aerial Vehicle (UAV).

I STAND-ALONE SENSING

The stand alone camera sensors system shown in **Figure 1 (c)** has been developed with a 4 bands MS4100, a multispectral charged couple device (CCD) camera (Geospatial), a pan/tilt device (PT570P medium duty) and receiver (LRD41C21/22 Legacy® and a lens

Figure 1 Field view and tower camera sensing platform in the University of Illinois at Urbana-Champaign

controller (Image Lab). The multispectral camera is a digital progressive scan camera with a high resolution of 1920x1080 pixels. In contrast to a normal CCD camera, the camera is available in two spectral configurations: RGB for high quality color imaging and color-infrared for multispectral applications. The camera has 3 CCD channels and channels have center wavelengths of 650nm, 800nm and 500nm, respectively and bandwidth of approximately 100nm for each. A serial interface provided external control of gain and exposure time for each independent channel via a standard RS 232 port. The gain settings control the amount of the output signal amplification for each individual channel in the camera. The gain of the camera ranges from 0dB to 36dB corresponding to 95 to 1023 in 16-bit digital number representation and 928 steps in total. Exposure time is the amount of time that each channel in the camera accumulates charge before the electronic shutter is closed and resulting value is read out. The exposure time of the camera varies from 0.1ms to 108 ms that corresponds to 16-bit digital number from 1 to 1080, 1079 steps in total. The maximum frame rate of the camera is 10 frames per second. The camera is able to output 8-bit and 10-bit digital image for each channel. The 8-bit mode and a digital frame grabber IMAQ PCI 1428 (National Instruments, Austin, TX) is used in the image acquisition process. The PCI 1428 is a highly flexible IMAQ board for PCI chassis that supports a diverse range of Camera Link-compatible camera. The PCI 1428 has been installed into an industrial small rugged computer with PCI expansion slot (SC241S) that can operate at extreme outdoor conditions. A serial port of the computer was connected to the external control port of the camera via a nine-pin serial cable. The pan/tilt device was rotated in horizontal and vertical directions to get the images according to the plot distributions. The Pelco D protocol was used to communicate with the pan tilt device and receiver using RS232 serial communication. The pan tilt rotates 0º-355º horizontally and 0º-90º degree vertically. The presets according to the field distribution are established using the caller identifications and automatic rotations of the pan/tilt device has been developed. A Nikon F mount variable zoom lens (17 mm- 200 mm) which was controlled by high precision motors and the lens controller was used to the precise movement of lens for zoom out and in (**Figure 1**). The lens motorization was developed externally and used two motors to control zoom and focus. The calibration was performed for zoom and focus of the lens using two potentiometers.

FIELD PLOTS DISTRIBUTION

The camera sensor system has been developed to capture images from 38 meter height tower for Miscanthus, switch grass, prairie grass and corn (**Figure 2**). The average plot size was 9 acres and stand alone tower was erected at the middle of the four fields. The perennial crops were at the first year of their growth and needed to replant rhizomes for uniform density of canopy. The perennial energy crop like Miscanthus requires 3 to 4 years to establish in a uniform pattern.

FIELD SURVEY AND MAP DEVELOPMENT

An RTK GPS-based field survey was completed and a 38-meter-tall tower was placed so that it could collect images of Miscanthus, switch grass and prairie grass across the entire field. The layout of the field is depicted in **Figure 2**. A laboratory-view, real-time algorithm was developed to capture images from the field over the growing season.

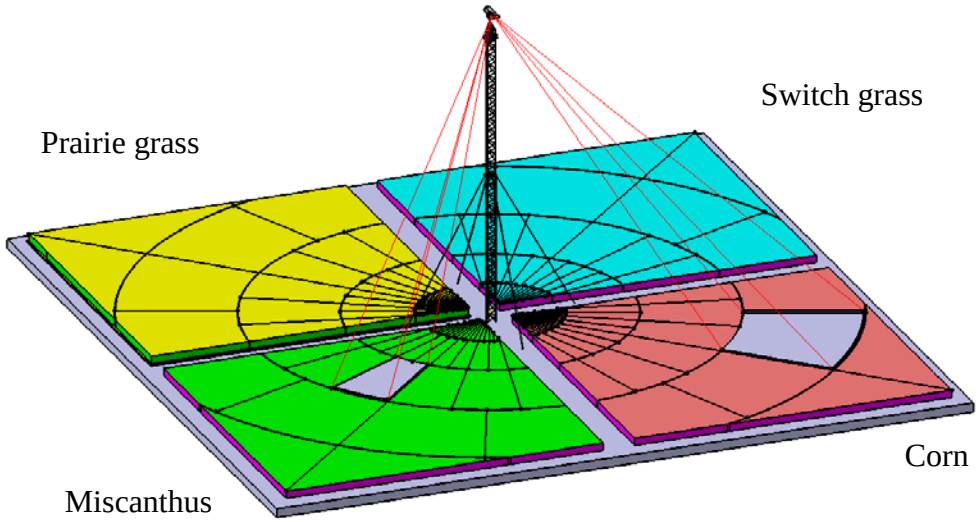

Figure 2 Field plots distribution and tower location at the energy farm, University of Illinois at Urbana-Champaign campus

Initially, twenty preset positions were created to cover each of the fields. A 50-mm fixed focal length was chosen to capture images. The NIR, red and green channels were averaged in the image acquisition process. An ArcGIS field plot shape file was prepared for further geo-referencing of images. Tower coordinates and GCP images were collected and surveyed using RTK GPS; coordinates are listed in **Table 1**. The geometrical arrangement of camera coordinates can be expressed as:

$$X_c = X_T + l_h \cos\alpha$$
$$Y_c = Y_T + l_h \cos\alpha$$

(X_c,Y_c) is the camera coordinates at the tower; (X_T, Y_T) is the tower position at the energy field, l_h is the length of the camera housing and α is the heading direction of the camera housing given by the digital compass (Sparton Electronics, SP3004D)

IMAGE GEO-REFERENCING

Camera model

A 2D point in an image is denoted by $m = [u, v]^T$, and a 3D point in the real world is denoted by $M = [X, Y, Z]^T$. The camera is modeled by the usual pinhole: the relationship between a 3D point in the real world and its projection point in the image is given by equation (1) (Zhang 2000):

$$s\begin{bmatrix} u \\ v \\ 1 \end{bmatrix} = A\begin{bmatrix} R & t \end{bmatrix}\begin{bmatrix} X \\ Y \\ Z \\ 1 \end{bmatrix}$$

where s is an arbitrary scale factor, (R,t) is the extrinsic parameters, which relates the world coordinate system and the camera coordinate system by rotation and translation. A is the camera intrinsic parameter matrix given by:

$$A = \begin{bmatrix} \alpha & \gamma & u_0 \\ 0 & \beta & v_0 \\ 0 & 0 & 1 \end{bmatrix}$$

with (u_0, v_0) is the coordinate of principal point, α and β are the focal length expressed in units of horizontal and vertical pixels, γ is a parameter describing the skewness of the two image axes. After considering the lens distortion, the camera model was decomposed and expressed in a different way. The lens distortion model was first introduced by Brown in 1966 (Brown 1971). Let $(\hat{x}, y)$ denote the ideal normalized image coordinate (distortion-free), and (x, y) denote the normalized image coordinate after applying distortion.

1) Normalization

$$\begin{bmatrix} u \\ v \\ 1 \end{bmatrix} = A\begin{bmatrix} x \\ y \\ 1 \end{bmatrix}$$

2) Distortion model

$$\begin{bmatrix} x \\ y \\ 1 \end{bmatrix} = \begin{bmatrix} (1+k_1r^2+k_2r^4+k_5r^6)\hat{x}+dx_1 \\ (1+k_1r^2+k_2r^4+k_5r^6)\hat{y}+dx_2 \\ 1 \end{bmatrix}$$

$$\begin{bmatrix} dx_1 \\ dx_2 \end{bmatrix} = \begin{bmatrix} 2k_3\hat{x}\hat{y}+k_4(r^2+2x^2) \\ k_3(r^2+2\hat{y}^2)+2k_4xy \end{bmatrix}$$

$$r = \sqrt{\hat{x}^2+y^2}$$

where k_1, k_2 and k_5 are called radical distortion coefficient; k_3 and k_4 are called tangential distortion coefficient.

3) Rigid motion

Without loss of generality, we assume the model plane is on $Z = 0$ of the world coordinate systems.

$$s\begin{bmatrix} \hat{x} \\ \hat{y} \\ 1 \end{bmatrix} = \begin{bmatrix} r_1 & r_2 & t \end{bmatrix}\begin{bmatrix} X \\ Y \\ 1 \end{bmatrix}$$

where r_1, r_2 and r_3 are the columns of rotation matrix R, t is the translational vector. From the equations above, we can notice that in order to transform between image coordinate and world coordinate, the camera intrinsic parameter matrix A, lens distortion model coefficient vector k, and the extrinsic parameter (R,t) need to be calibrated.

Camera intrinsic parameters calibration

A lab calibration was performed to calibrate camera intrinsic parameters and lens distortion coefficient. A model panel containing 11×11 pattern squares was used.

The size of the pattern is 30mm×30mm. It was printed with a high quality printer and pasted on a flat board. Twenty images of the model plane were captured form different orientation. All of them were used to calibrate the intrinsic parameters and lens distortion coefficient. After calibration, all the corners were re-projected back through the intrinsic parameters calibrated for error analysis purpose. The parameters *kc*(1), *kc*(2) and *kc*(5) are the coefficients of the round distortion model, and *dx* is the tangential distortion vector. Therefore, the 5-vector '*kc*' contains both radial and tangential distortion coefficients.

Transfer Matrix

The transfer matrix relates the ground coordinate to the image coordinate. It was composed of the extrinsic parameters, including three angles of the camera and the distance from camera to ground and this can be determined using a digital compass.

$$x_{cam\_frame} = T_{transfer} \cdot X_{ground}$$

where, x_{cam_frame} is the coordinate in the camera reference frame, and X_{ground} is the corresponding coordinate of the ground. There are generally two parts in the transformation process: rotation (R) and translation (T). Then the relationship between two coordinates can be expressed by:

$$x_{cam\_frame} = R \cdot (X_{ground} + T)$$

$$R = \begin{bmatrix} \cos\theta\cos\psi & -\cos\phi\sin\psi + \sin\phi\sin\theta\cos\psi & \sin\phi\sin\psi + \cos\phi\sin\theta\cos\psi \\ \cos\theta\sin\psi & \cos\phi\cos\psi + \sin\phi\sin\theta\sin\psi & -\sin\phi\cos\psi + \cos\phi\sin\theta\sin\psi \\ -\sin\theta & \sin\phi\cos\theta & \cos\phi\cos\theta \end{bmatrix}$$

$$T = \begin{bmatrix} 0 \\ 0 \\ h \end{bmatrix}$$

Where R is the rotation matrix, which represents the angles between the camera reference frame and the ground. θ, Φ, and ψ are the yaw, pitch, and roll of the digital compass and T is the translation matrix, which represents the position difference of camera and the origin of the ground coordinate. Considering, the origin of the ground coordinate is the position of the tower center projection on the ground, then T has the form [0 0 h]' where h is the distance from the camera to the ground, or the height of the tower.

SPATIAL RESOLUTION AND FOCAL LENGTH

Spatial resolution was the first variable to be considered because it largely determines how much detail could be interpreted on the final image and numbers of images were needed to be captured. The spatial resolution can be defined as how much area is represented by a pixel on the image sensor. The spatial resolution must be large or small enough to meet the objectives of the application requirements. There are three major factors that influence the spatial resolution. First, the tower height; second is the focal length of the sensor; and third is the tilt angle of the camera with the vertical plane. The relationship among those three variables can be expressed as following equation (Paine and Kiser, 2002).

$$R = \frac{S_{pixel} * \sqrt{(h^2 + l^2)}}{f}$$

$$l = h \tan \alpha$$

Where R is the spatial resolution; S_{pixel} is the pixel size of the image sensor; H is the height of the tower, (38.1 m); f is the focal length; R is spatial resolution; s is the pixel size of the camera, (7.4×7.4 micron); L is the ground distance to the tower center (0 to 268 m) and f is the focal length of the lens (16-160 mm).

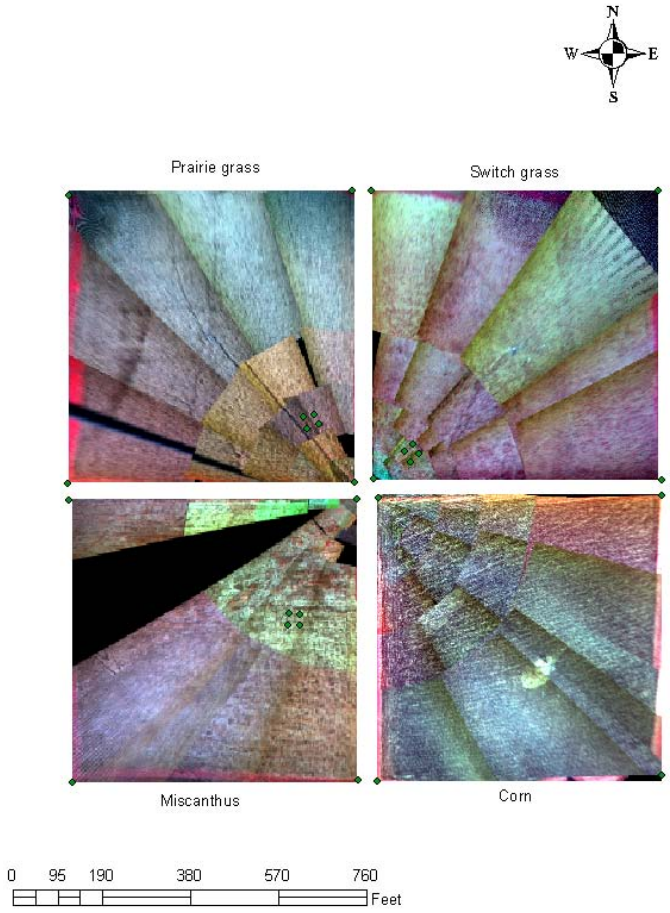

Figure 3 Ortho-rectification and mosaic of CIR images captured from stand alone remote sensing system for Miscanthus, corn, switch grass and prairie grass

IMAGE ACQUISITION ALGORITHM

The image acquisition and positions for camera was placed based on yaw and tilt angle from pan tilt device. The compass was used to get the yaw and tilt at every preset position. The automatic image acquisition was developed to get the images at any time. The caller for each of the point can be marked. The real-time monitoring either snapping or grabbing of image was captured. The Labview® 8.0 was used to develop image acquisition and monitoring for multi-spectral camera. The image was captured with the information of date, time, position, yaw and tilt and image type. The temporal resolution was the major advantages for image database. For ground based sampling, in the plots, four 8 m x 8m ground reference points were selected to keep tracking the vegetation indices and intercepted solar radiation for the canopy.

ORTHO-RECTIFICATION AND MOSAIC OF IMAGE

The image was captured in an oblique view from tower and ortho-rectified using geometrical coordinate transformation and transfer matrix (**Figure 3**). The RTK GPS was used for geo-referencing of mosaic image based on control points. The Arcview GIS® 9.3 was used to prepare the geo-reference image. The raster was projected on NAD1983 and GCS coordinate for the energy farm. The natural featured were considered for the geo-reference of image. Ortho-rectification was done in a post processing of image using Matlab image processing toolbox. ERDAS Imagine and Arcview GIS were used for spectral analysis. Mosaic and ortho-rectification of image shows the site-specific position of each of the plot. The spatial resolution after mosaic and geo referencing was 12 cm per pixel.

II GROUND REFERENCE DATA COLLECTION VEICLE (DAV)

The Data Acquisition Vehicle (DAV) described here was intended for crop monitoring, sample acquisition, weed control, and chemical application. The vehicle employs 4-Wheel-Drive-4-Wheel-Steering (4WD4WS) locomotion and uniquely embraces two- degrees-of-freedom (2DOF) reconfigurability in terms of clearance and wheel gauge.

LOCOMOTION

The operating environment of the DAV would be in dense and high crops, in a *Miscanthus* field. High clearance and the requirement to minimize damage of plants were the challenges over the traditional tractor driving locomotion. Nevertheless, design complexity and power consumption are increased while the individual leg mechanism would be employed. Therefore, a combination of multi-wheeled and multi-legged locomotion is the ideal choice for our application. This is critical for improving the mobility, trafficability, and maneuverability as well. Hence, wheel-legged locomotion with a 4WD4WS mechanism has been selected as the basic configuration of the DAV locomotion. To achieve the locomotion selected, eight motors in this platform, four drive motors and four steer motors, have been proposed. Selecting the right motor usually is the first step of a motorized robotic system. The detailed mathematical model has been reported on Xiong et al 2009.

SYSTEM DESIGN

The system was designed to use devices that are readily available on the market for either small scale weeding applications or manually-pushed data collection applications. The vehicle has high clearance and adjustability and is self-propelled. It consists of four legs, a chassis framework, an operating arm, and a generator for power supply. Each leg unit is capable of lifting, steering, and driving.

Drive Module

The DAV employs a wheeled-legged mechanism in which adjustable legs are used for lifting up and down and for turning the wheels in order to widen or shorten the wheel gauge. 2DOF adjustability is achieved in a large, semi-autonomous platform. To drive the wheel freely or to disconnect the wheel from the drive chain when necessary, this drive unit has two adjustable positions: engaged and disengaged. Details of the drive module are depicted in **Figure 4**. Two pillow blocks are mounted in the bottom two ends of the drive yoke (1) to horizontally hold the drive shaft (2) and the core of the drive module.

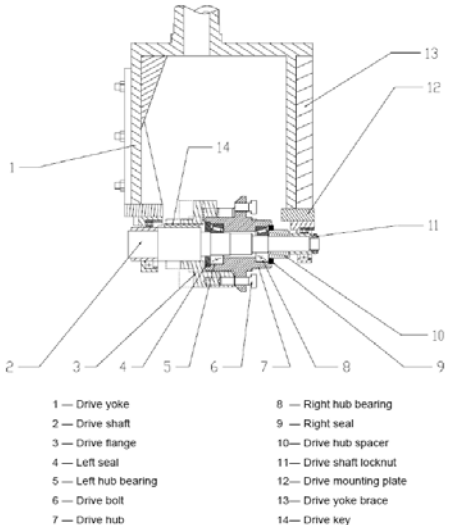

(4)

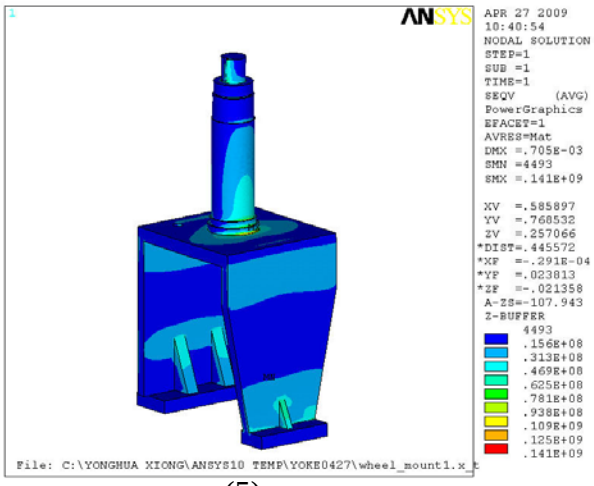

(5)

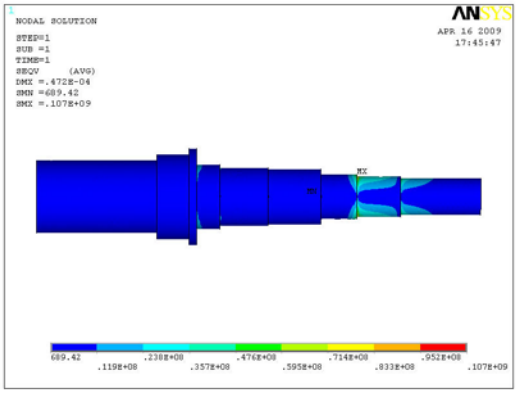

(6)

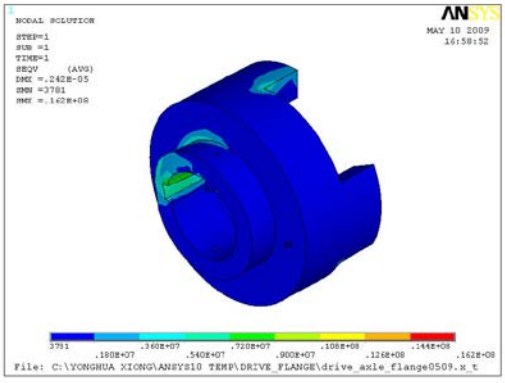

(7)

Figures (4) Drive module; (5) The FEA result of yoke; (6) The FEA result of drive axle and (7) The FEA result of drive flange

drive module is depicted in Figure 7. In the bottom two ends of drive yoke 1, two pillow blocks are mounted, horizontally holding the drive shaft 2, the core of the drive module.

***Engaged and disengaged position*:**

As shown in the solid-line profile, the drive flange (3), which can be driven by the drive shaft through the drive key and can be engaged with the drive hub and the wheel, is mounted at this point. The wheel can be driven synchronously with the drive shaft as the claw-shaped flange meshes with the six gussets around the drive

hub. When the drive flange slides away from the hub to the dashed-line position, the entire drive chain can be cut off, and the wheel can be rotated freely with the hub. A series Finite Element Analysis (FEA) was completed for the key components. FEA results in **Figure 5-7** show that they were safe even in a severe working environment. The maximum stresses of the three key components were 141 MPa, 107 MPa, and 16.2 MPa separately, which are far less than the allowable stress [δ] (207.5 MPa).

Table 2. Section FEA analysis results

Type of section	Round		Rectangular		User-defined	
Reinforcement	Braced	W/O	Braced	W/O	Braced	W/O
Maximum stress (Mpa)	26.1	42.0	62.8	98.6	23.8	48.5
Weight (Kg)	460.9	421.0	376.2	338.1	312.6	289.4
Cost (USD)	1,581	1,357	1,495	1,420	2,100	1,950

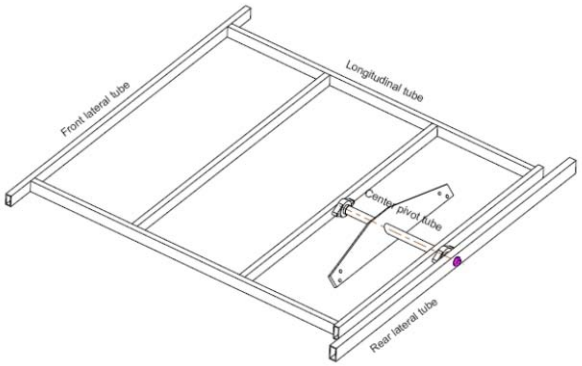

Figure 8 Three types of section compared gauge

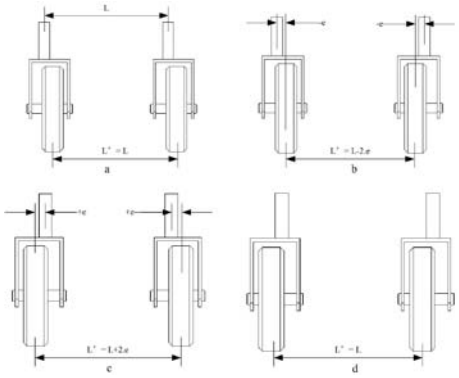

Figure 9 Different layouts of wheel

For detailed investigation, the maximum stress of yoke occurred at the neck circle where the steering mechanism is located, because the whole dynamic weight is distributed down to the wheel through this circle. The ultimate stress point of the drive axle occurred at the second smallest shoulder that fit with the support bearing of drive hub. This is reasonable, as the shaft diameter there is smaller than the other support bearing, while holding equal weight. The keyway on the flange is in the weak area, where the drive shaft transmits torque (**Figure 4**). The torque turns, delivers to the flange and eventually to the driving wheel.

Chassis Frame

This section describes the proposed chassis structure. A rotating DOF along the longitudinal axis is essential for adapting to sloped terrain with four wheels touching the ground. Therefore, the rear lateral tube was designed to pivot around a central, round tube through a joint at the intersection. The lightweight design has been optimized for finite element analysis by comparing three types of sections; make sure all four wheels are touching the ground at any time, a rotating DOF by the longitudinal axis is essential. Hence, we designed the rear lateral tube to be pivoted with a center round tube through a joint at the intersection. The arrow shows the rotating directions can provide. Lightweight design is optimized by comparing three types of sections, as shown in **Figure 8**. The results and comparisons are listed in Table 2. The safest option is to employ the user-defined section bar, ignoring the cost, while the round section tubing is the heaviest frame among the three sections. Comparatively, the rectangular tubes could be the optimum choice, considering both strength and weight factors. The tensile stress is 270 MPa, which is around three times higher than the maximum stress of

rectangular tubing; thus, the choice is the lightest frame we can get, in order to meet the lightweight design goal with enough strength. As previously mentioned, DAV has been developed with the ability to adjust the configuration to adapt to the different operating environment of a *Miscanthus* field. For the adjustable lifting mechanism, two square tubes sliding each other through the guide of two bushings has been selected. To avoid the damage of crops that have expanded out to the intra-row, the wheel gauge of DAV needs to be changeable, following the certain track of empty intra-row space. The gauge can be reconfigured in several layouts, as arranged in **Figure 9**. Letting the leg distance in lateral axis be L (**Figure 9a**), we can arrange four wheel gauge layouts by the offset (e) on each drive module. Keeping the left wheel straight forward and turning the right wheel 180 degrees will make the wheel gauge change from L to L-2e, as shown in **Figure 9b**. When the left wheel is rotated 180 degrees, while keeping the right wheel with the positive offset (+e), the gauge is adjusted to L+2e (**Figure 9c**). The fourth layout (**Figure 9d**) is the opposite of the layout (a), sharing the same gauge value.

FABRICATED DAV AND SENSING SYSTEMS

All the drive modules, steering modules, lifting leg units, the chassis frame and operating arm has been assembled, and the completed unit is shown in **Figure 10** and **11**. Particularly, the overall specifications: Locomotion 4WD4WS, Length 3., Width 3.2 m, Height 3.1-4.1, Weight 1500 kg, Clearance 3-4 m, Wheelbase 3.1 m, Wheel gauge 2.85,3,3.15 m, Speed 1 m/s, Maximum traction 7812 N, Maximum steering torque 130 N.m, Turning radius 0 m, Operating time 10 hr, power supply 6.5 kW The DAV system is a Mobile Crop Monitor and Data Collector. The remote sensors would be equipped on the DAV. A frame of remote sensing images can be collected which covers a small area around this point. The running path and control points of DAV are decided to cover the field and crops (**Figure 12)**. The DAV could be able to sense in a close proximity of crops. DAV platform can be controlled either automatically or manually. The navigation path and control points can be stored as pre-set path and DAV can be control autonomously and the data can be collected. The vehicle has been design to control in real-time and operated from joystick either at ground station or onboard. The control system of the DAV should has been designed. Carefully and the DAV could be controlled either with or without the

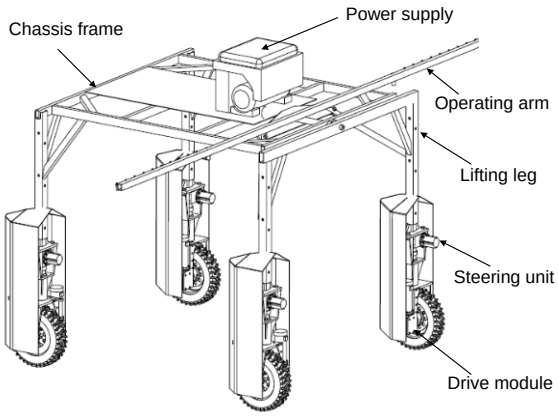

Figure 10 CAD solid model of R-DAV

Figure 11 Fabricated Model of R-DAV

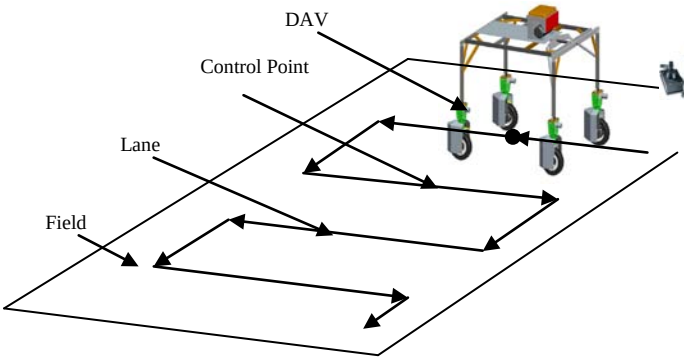

Figure 12 Proposed Path tracking pattern

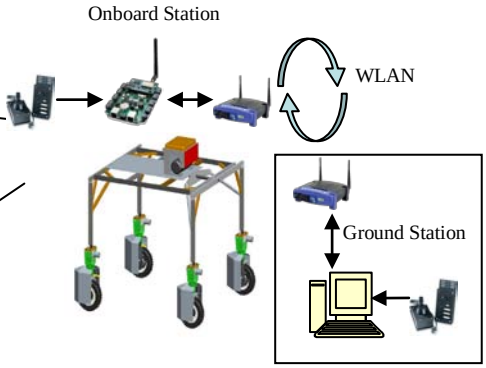

Figure 13 Onboard and ground station of DAV

ground station. The structure of DAV control system has been designed as a Field Bus Control System (FCS) model. This system has two structure levels: the onboard - ground station (**Figure 13**). These two levels are linked by long rang wireless communication. The ground station is the most convenient way to use the DAV. It provides the interface between DAV and operators. Image acquisition for crop over the growing season can be collected. The onboard level control subsystem is mainly communicated with the controller on the vehicle. The structure of the onboard control subsystem has been designed according to a star topology network (**Figure 14**). It included a DAV body micro controller and four LEG micro controllers

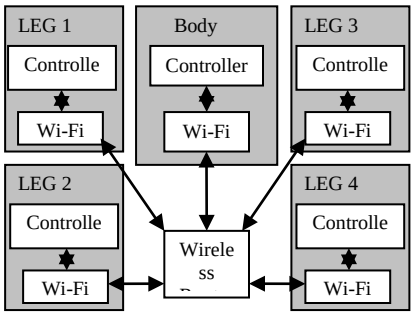

Figure 14 Star topology networking distribution

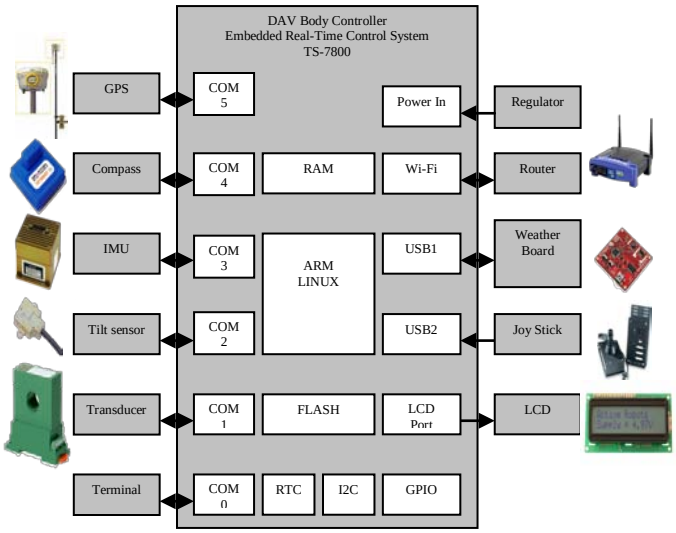

Figure 15 Communication and sensors

The DAV body controller is an ARM-Linux-based, embedded, real-time control system, which is more powerful than an LEG controller (**Figure 16**). It receives commands from the ground station or joystick and determines the behavior of the DAV as well as the sensors. The RTK-GPS, DMU, digital compass and tilt sensor are linked to the body

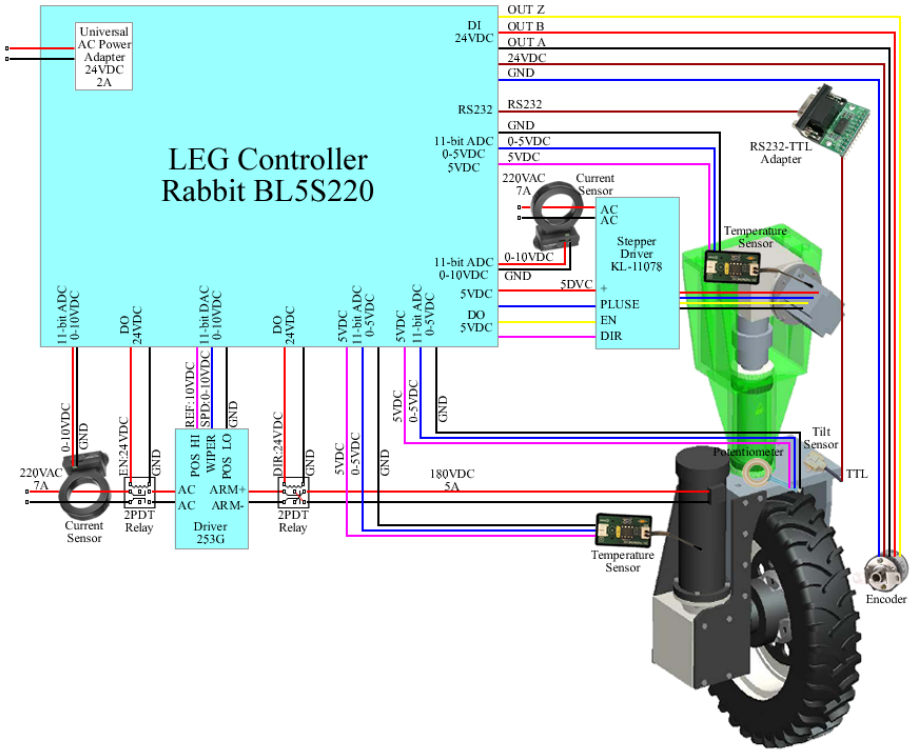

Figure 16 LEG controller and sensors communication

controller to detect the posture of the vehicle. A voltage/current transducer is used as a power consumption monitor. Weather sensors detect the relative humidity, temperature, barometric pressure and light stress in the field. The basic input and output devices for onboard operation are a joystick and an LCD panel, respectively. Remote sensors for installation on the DAV are selected based on application requirements, and may include a hyperspectral meter and/or other newly developed sensors. Due to the selection of 4WD4WS mechanics and real-time vehicle control, dividing the total control load into four legs with dedicated controllers is appropriate for this application. Each LEG controller provides Direct Digital Control (DDC) for the motor, stepper and sensors. The PID algorithm effectively controls both driving speed and steering direction. Temperature sensors protect the system from overheating. Current transducers monitor motor power consumption and any overload information. Importantly, tilt sensors can detect the deformation of the joint between the leg and the body; this deformation should be small in order to prevent damage to the stiff, 3-m-high, steel frame structure. The vehicle control mode can be set to either automatic or manual, and the steering mode of the 4WD-4WS DAV can be selected from the following: 1) front Ackerman Mode (car-like mode), 2) Rear Ackerman Mode, 3) Double Ackerman Mode, 4) Omni Mode, 5) Point Turn Mode, and 6) Breaking Mode.

III UNMANNED AERIAL VEHICLE (UAV)

This research was aimed to develop an UAV based agricultural remote sensing system to provide a maximum flexibility in crop image collection (**Figure 17**). Specific first objective of this research was to develop a ground base station for the UAV system for mission planning, flight command activation and flight monitoring.

Figure 17 Unmanned Aerial Vehicle (UAV) to Monitor Energy Crop

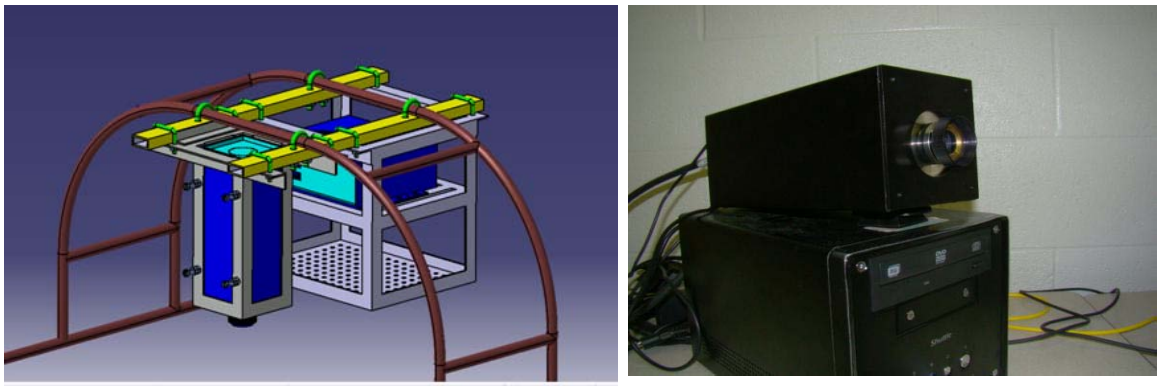

Figure 18 CAD design of camera position and hyperspectral sensor

The second was to develop a navigation system for the UAV using IMU sensors, GPS and sensor fusion techniques to directly determine the accurate position and attitude of the UAV from physical sensor measurements. The navigation system can be controlled by the ground station, and able to navigate the UAV to reach the predefined waypoints.

UAV HARDWARE COMPONENTS

The UAV system hardware mainly consists of an RC helicopter, a hyperspectral-spectral camera (**Figure 18**), an IMU, a WAAS differential-corrected GPS, a single board computer (SBC), a flight controller, a PWM switch, a wireless router and a video transmitter. The helicopter is a commercially available model helicopter designed and produced by Rotomotion Inc. that uses a twin cylinder

Bergen/Zenoah – 52 cc engine, which produces about 8 hp. It is capable of lifting a 25-lb payload for 30 to 45 minutes on a tank of gas. An Autonomous Flight Control System (AFCS, Rotomotion, SC) was mounted on the helicopter. The AFCS is an integrated package designed to control and guides an R/C-class helicopter with a weight of 1.25 lb. It was uniquely tuned for the airframe and used to generate servo commands according to the flight status from a navigation system. A 12 V battery and generator are used as double power supplies to run the whole helicopter system. A high-resolution hyperspectral-spectral camera from SpecIR was chosen as the image sensor (**Figure 18)**. The ADC utilizes a single 3.2 million (2048 x 1036) pixel CMOS sensor to sense green band (520 nm - 620 nm), red band (620 nm - 750 nm), and near-infrared (750 nm - 950 nm) images. The camera provides 8-bit radiometric resolution and gives digital counts in the range between 0 and 255 per channel.

CONCLUSIONS

A stand-alone remote sensing system was developed to monitor energy crops. The advantage of this stand-alone system is its capacity to record the spatial and temporal variations in crop growth patterns over the growing season. The image acquisition system, image mosaic, and geo-referenced map were developed in a GIS environment to facilitate site-specific management of energy crops. A Ground Reference Data Acquisition Vehicle (DAV) and an Unmanned Aerial Vehicle Platform were also developed. Additional experiments and real-time processing methods will be used to determine the optimum harvest time for energy crops based on intercepted photosynthetically active radiation.

REFERENCES

Bajwa SG and LF Tian 2005, Soil Fertility Characterization in Agricultural Field Using Hyperspectral Remote Sensing, Transaction of the ASAE, 48(6):2399-2406

Brown DC, Close Range Camera Calibration, Photogrammetric Engineering, 1971, 37:855-866

Paine, D. P., and J. D. Kiser. 2002. *Aerial Photography and Image Interpretation 2nd Edition*. New York, N.Y.: John Wiley and Sons.

Ting KC, A., Hansen, Q. Zhang, T. Grift, L. Tian, S. Eckhoff, and L. Rodriguez 2008, *Engineering Solutions For Biomass Feedstock Production,* http://www.energybiosciencesinstitute.org

Xiong, Y, L. Tian, T. Ahamed, F.A.C. Pinto, B. Zhao. A reconfigurable data collection vehicle for bioenergy crop sensing and management. 4th IFAC International Workshop on Biorobotics, Information Technology and intelligent control for Bioproduction System, September 9-11, 2009**,** Champaign, Illinois, USA

Zhang, Z.. A Flexible Camera Calibration By Viewing a Plane From Unknown Orientations. *IEEE Trans. on Pattern Analysis and Machine Intelligence.* 2000, 22 (11):1330-1334

+